CD300e Controls Macrophage Lipid Handling and Safeguards Adipose Tissue Function in Obesity

Sara Coletta[1*], Simone Pizzini[1], Stefania Vassallo[1], Elisabetta Trevellin[2], Annica Barizza[1], Sofia Giacometti[1], Gabriele Sales[1], Fabrizia Carli[3], Amalia Gastaldelli[3], Roberto Vettor[4,5], Marina de Bernard[1*]

[1]Department of Biology, University of Padova, Italy

[2]Medical Clinic III, Department of Medicine (DIMED), University of Padova, Padova, Italy

[3]Cardiometabolic Risk Unit, Institute of Clinical Physiology, National Research Council-CNR, Pisa, Italy

[4]Department of Medicine (DIMED), University of Padova, Padova, Italy

[5]Center for Metabolic and Nutrition Related Diseases - Humanitas Research Hospital Rozzano, Milano, Italy

*Correspondence: Sara.coletta@unipd.it (S.C.), marina.debernard@unipd.it (M.d.B.)

Abstract

In obesity, adipose tissue macrophages (ATMs) cluster around hypertrophic adipocytes, where they actively engage in lipid uptake, lysosomal degradation, and fatty acid metabolism. Emerging evidence indicates that lysosomal dysfunction within ATMs exacerbates lipid retention, promoting the release of anti-lipolytic factors that suppress adipocyte lipolysis and perpetuate adipose dysfunction.

In this study, we uncover a previously unrecognized role for the immune receptor CD300e in this regulatory network. Using a *Cd300e*$^{-/-}$ mouse model under high-fat diet conditions, we demonstrate that loss of CD300e exacerbates adipocyte hypertrophy, aggravates hepatic steatosis, and impairs glucose and insulin tolerance. Mechanistically, CD300e-deficient ATMs exhibit increased lipid accumulation, while adipocytes shift toward enhanced lipogenesis and reduced lipolysis.

These findings advance our knowledge on immunometabolic crosstalk governing metabolic homeostasis within adipose tissue and identify CD300e as a critical sensor modulating lipid handling in ATMs, thus maintaining the metabolic dialogue between these cells and adipocytes. The absence of CD300e destabilizes adipose homeostasis, driving adiposopathy and systemic metabolic dysfunction. Therapeutically, targeting CD300e may represent a novel strategy to restore adipose tissue function and combat obesity-related metabolic complications.

Introduction

Obesity is recognized as a multifactorial chronic disease in which structural and functional modifications of adipose tissue (AT) have been recognized as the major trigger for the development of its complications [1–4]. Adiposopathy is the result of an immuno-metabolic derangement including a dysfunctional adipocyte, immune cells infiltration and inflammation with the development of fibrosis and its consequences at the level of the whole body. The interplay between metabolism and immunity has deep phylogenetic and ontogenetic origins, as evidenced by *Drosophila melanogaster*, where the fat body simultaneously performs immune functions and serves as a key metabolic organ, analogous to both adipose tissue and the liver in mammals [5].

When the metabolic microenvironment changes due to obesity or excess lipids, quantitative and functional changes of innate immune cells occur along with the secretion of adipokines and pro-inflammatory cytokines that modulate the local microenvironment, promote insulin resistance, induce hyperglycaemia, and activate inflammatory signalling pathways. Many immune cells in AT have been described as participating in obesity-associated inflammation, among them macrophages constitute a large proportion.

Recent advances in single-cell RNA sequencing technologies have unveiled the remarkable heterogeneity of adipose tissue macrophages (ATMs), the most abundant immune cells in expanded white adipose tissue (WAT). Rather than conforming to the traditional M1/M2 paradigm, ATMs exhibit a diverse range of phenotypes and functions that are significantly altered in obesity[6,7]. This phenotypic diversity has been observed in both humans and mouse models, although the relative abundance of ATM subtypes may vary across species[8,9]. Mounting evidence highlights the critical crosstalk between adipocytes and ATMs as a key regulator of adipose tissue homeostasis, inflammation, and obesity-induced metabolic dysfunction[10]. In obese conditions, ATMs accumulate in WAT and cluster around enlarged adipocytes, forming characteristic crown-like structures (CLSs). These lipid-laden ATMs show transcriptional signatures enriched in pathways associated with lipid

uptake, lysosomal biogenesis and function, and lipid metabolism, including mitochondrial β-oxidation. They are commonly referred to as lipid-associated macrophages (LAM)[11]. Under physiological conditions, adipocytes release fatty acids (FFA) and glycerol to support systemic energy demands, a process dependent on neutral lipases. Among these, adipose triglyceride lipase (ATGL) catalyzes the initial and rate-limiting step of lipolysis[12]. Once released, FFA can enter the bloodstream and taken up by peripheral tissues like liver, heart, and skeletal muscle. In addition, FFA can be locally engulfed by macrophages and processed through distinct metabolic pathways: β-oxidation for energy generation, esterification into triacylglycerols (TAG) for lipid storage, or cellular export[13]. In addition to canonical lipolysis, lipids are released from the adipose tissue through a lipase-independent pathway[14]. Indeed, adipocytes can secrete extracellular vesicles enriched in neutral lipids, termed adipocyte-derived exosomes (AdExos). Likely originating from multivesicular endosomes[15], these vesicles carry substantial amounts of TAGs and monoacylglycerols[14] and display elevated levels of various sphingomyelin species[16]. AdExos serve as a local lipid reservoir for ATMs and are central to a dynamic paracrine lipid exchange system: adipocytes release TAG-laden AdExos, which are internalized by ATMs via macropinocytosis, hydrolyzed intracellularly, and subsequently returned to adipocytes as FFA for re-esterification.

This tightly regulated cycle becomes markedly intensified in obesity, placing a considerable burden on ATMs—particularly those within CLSs—to process large volumes of lipids.

While CD36 , a cell surface scavenger receptor abundantly expressed in macrophages as well as non-immune cells such as adipocytes[17,18] plays a pivotal role in lipid fuel partitioning and channelling to both adipocytes[19,20] and macrophages[18], the mechanisms governing the internalization of TAG-rich AdExos remain poorly defined. Emerging candidates include members of the CD300 receptor family—immune cell-surface receptors that transmit inhibitory or activating signals[21,22]. These receptors are capable of recognizing a range of lipid ligands, including sphingomyelin, ceramide, phosphatidylserine, and phosphatidylethanolamine[21–23], positioning them as potential regulators of lipid-sensing and immune-metabolic responses.

Among them, CD300e has garnered attention for its potential role in adipose tissue remodelling. Its expression is upregulated in WAT from obese individuals and downregulated following weight loss[24–26], suggesting a sensitivity to metabolic status. Furthermore, the ability of CD300e to bind sphingomyelin[22]—a lipid abundant in AdExos[15]—raises the intriguing hypothesis that CD300e may mediate the uptake of TAG-enriched vesicles by ATMs, contributing to a compensatory mechanism during obesity progression.

In this study, we leverage a *Cd300e* $^{-/-}$ mouse model to investigate the functional role of this immune receptor in the interplay between adipocytes and ATMs, and its impact on obesity-driven adipose tissue remodelling and systemic glucose homeostasis.

Results

The obese adipose microenvironment drives CD300e induction during monocyte-to-macrophage differentiation

The finding that CD300e mRNA levels were elevated in the adipose tissue of individuals with obesity prompted us to investigate whether this increase reflected higher surface expression of the receptor on individual ATMs, rather than simply being a consequence of greater infiltration of these cells into the tissue. To this end, we isolated the stromal vascular fraction (SVF) from subcutaneous adipose tissue (SAT) samples collected from individuals undergoing lipectomy during abdominoplasty after bariatric surgery-induced weight loss, as well as from lean control subjects. ATMs were identified within the SVF as $CD11b^{+}CD68^{+}$ cells and subsequently analyzed for CD300e expression. As shown in Figure 1A, a higher percentage of ATMs from formerly obese individuals expressed CD300e compared to those from lean subjects. Moreover, the mean fluorescence intensity (MFI) of CD300e was significantly greater in the obese group (Figure 1B), suggesting enhanced receptor expression per cell.

Given that most ATMs originate from infiltrating monocytes, and that monocyte recruitment increases with adipose tissue expansion[27–29], we then assessed whether circulating monocytes from the two cohorts differed in CD300e expression. Consistent with previous findings, we confirmed that intermediate ($CD14^{+}CD16^{+}$) and non-classical monocytes ($CD14^{-}CD16^{+}$) exhibit slightly higher expression levels of CD300e compared to classical subset ($CD14^{+}CD16^{-}$) [30]. However, no significant differences in CD300e surface expression were observed across any monocyte subtypes between subject with obesity and lean individuals (Figure 1C). These findings suggest that CD300e upregulation occurs locally, likely induced by microenvironmental signals within the adipose tissue, during the differentiation of recruited monocytes into tissue-resident macrophages. In accordance, conditioned media collected from freshly isolated vascular fraction of obese SAT triggered the expression and the exposure of CD300e in monocytes (Figure 1D and E).

CD300e prevents the adipocyte hypertrophy induced by excessive energy intake

Before conducting a detailed investigation on the role of CD300e in obesity-driven adipose tissue remodelling and glucose homeostasis taking advantage of a knockout (KO) mouse model generated by the deletion of exon 2 of the *Cd300e* gene[31] (Figure 2A), we first assessed whether the upregulation of CD300e observed in adipose tissue of obese humans was also recapitulated in mice fed a high fat diet (HFD). Wild type (WT) mice of the C57BL/6 strain at the age of 8 weeks were fed a HFD ad libitum for 16 weeks, while control WT mice were fed chow diet (CFD).

Epididymal (VAT) and subcutaneous inguinal (SAT) fat pads were collected. Figure 2B shows that, like observations in humans, obese mice exhibited increased expression of *Cd300e* mRNA in VAT. These findings support the use of mice as a relevant model to study the role of this immune receptor in the context of obesity.

We investigated whether CD300e up regulation was part of a positive feedback loop activated by body mass gain to mitigate the harmful effects of overnutrition. To accomplish this, we utilized *Cd300e*-null mice subjected to a HFD and compared their phenotype to that of WT controls. There was no notable difference in body weight between WT and *CD300e*$^{-/-}$ mice under standard conditions (Figure 2C). However, following HFD feeding, *Cd300e*$^{-/-}$ mice exhibited significantly greater body weight than their WT counterpart, with differences emerging as early as 6 weeks into the HFD regimen (Figure 2C).

VAT were collected from all animals upon completion of the diet regimens. Macroscopic comparison of the specimens indicated that *Cd300e*-null mice fed a HFD had a bigger mass than their WT counterparts subjected to the same diet (Figure 2D right panel). In accordance, while VAT weight was comparable between WT and *Cd300e*$^{-/-}$ mice fed a CFD, it was significantly increased in HFD-fed null mice compared to WT counterparts (Figure 2D, left panel). H&E staining revealed considerable enlargement of adipocytes in *Cd300e*$^{-/-}$ mice under HFD feeding, with quantification of the cross-sectional areas confirming adipocyte hypertrophy (Figure 2E). All the observations made on VAT were recapitulated in the subcutaneous inguinal one (SAT, Figure 2F-G).

CD300e prevents liver steatosis and glucose dysmetabolism during obesity

Given the strong accumulation of lipids in the liver during obesity and the close association between adiposity and metabolic dysfunction associated steatotic liver disease (MASLD) in humans[32], we extended our analysis to this organ. The liver weight (data not shown), and histological appearance (Figure 3A), of mice were comparable between the two genotypes in CFD. However, under HFD, the weight of liver from *Cd300e*$^{-/-}$ animals was higher than that of their WT counterparts (data not shown). Consistently, *Cd300e*$^{-/-}$ mice fed a hypercaloric regimen exhibited more severe hepatic steatosis compared to WT mice (Figure 3A). In accordance, total amount of TAG was higher in *Cd300e*$^{-/-}$ versus WT livers (Figure 3B) and this was confirmed by lipidomic analysis that revealed that about 60% of major TAG species were increased in null mice (Figure 3C).

To determine the metabolic consequences of *Cd300e* ablation, we conducted glucose tolerance tests (GTT) and insulin tolerance tests (ITT) in both *Cd300e*$^{-/-}$ and WT mice on a CFD and HFD. In CFD mice, the deficiency of *Cd300e* did not alter glucose levels compared to WT, in both GTT and ITT (Figure 3D-E). However, when HFD mice were challenged with an intraperitoneal glucose bolus, blood glucose levels were significantly higher in *Cd300e*$^{-/-}$ mice at 60, 90, and 120 min after the administration of the bolus compared to WT mice. Similarly, when HFD mice were injected with insulin, *Cd300e*$^{-/-}$ mice displayed higher blood glucose levels than WT mice at all time points, with significant differences at 15, 30, and 60 min after the hormone injection (Figure 3D-E). Furthermore, while the basal level of glucose, measured after a 5-hour fasting period, was comparable between WT and *Cd300e*$^{-/-}$ mice on CFD, *Cd300e*$^{-/-}$ mice exhibited significantly higher glucose concentrations compared to WT animals on HFD (Figure 3F).

Considering that CD300e is expressed almost exclusively by myeloid cells[33], excluding neutrophils, we generated a conditional KO mouse lacking expression in the myeloid lineage[31] to confirm that the observed effects were specifically due to the absence of CD300e in myeloid mononuclear cells. The results obtained using the conditional mutant closely mirrored those observed in the full KO mice (Supplementary Figure 1).

Cd300e$^{-/-}$ mice lack significant adipose tissue inflammatory response

The production of proinflammatory molecules by adipose tissue is thought to contribute to obesity-related metabolic complications, including insulin resistance and type 2 diabetes[34]. Macrophage accumulation in WAT is a hallmark of obesity-related inflammation[7,11,27]. However, T cells also undergo both numeric and phenotypic changes in obesity and have been implicated in obesity-induced insulin resistance and systemic inflammation[35].

Therefore, we investigated whether the glucose dysmetabolism observed in *Cd300e*$^{-/-}$ mice might be accompanied by exacerbated adipose tissue inflammation compared to WT animals, as might be expected given the extensive tissue remodelling in the absence of the gene.

Consistent with published findings, we confirmed that diet-induced obesity in WT mice led to an increased proportion of macrophages (F4/80^{+} cells), as well as CD4^{+} and CD8^{+} T cells in VAT, compared to chow-fed controls (data not shown). In *Cd300e*$^{-/-}$ mice, the percentage of these cells raised further (Figure 4A). However, the pro-inflammatory cytokines IL-6, TNF-α, and IL-1β did not exhibit any relevant difference in terms of up-regulation between the two genotypes, either in VAT (Figure 4B), or in macrophages purified from VAT (Figure 4C). We found largely similar findings when we extended the investigation to SAT (Supplementary Figure 2).

Collectively, these data argue against a substantial contribution of inflammation to the worsened dysmetabolism associated with the extensive adipose tissue remodelling observed in the absence of the immune receptor.

Single-cell analysis of adipose tissue immune cells from KO mice reveals that adipose tissue macrophages exhibit a transcriptional profile reminiscent of LAMs

The crucial role of ATMs in the homeostasis of adipose tissue and metabolism is supported by the phenotype that animal models exhibit when they are deficient for genes related to their role as lipid

handlers. For example, the deficiency of the lipid receptor TREM2 is accompanied by dysfunctional adipose tissue with adipocyte hypertrophy, dyslipidemia, exacerbated HFD-induced weight gain and worse systemic glucose tolerance. Such a phenotype relies on the abrogation of lipid uptake and storage in *Trem2*$^{-/-}$ macrophages due to the lack of most of the LAM gene signature[10].

Based on this evidence and on our findings, we reasoned about the possibility that the absence of CD300e could compromise the acquisition of LAM profile by ATMs in obese *Cd300e*$^{-/-}$ mice. To test this hypothesis, we conducted a more detailed characterization of the immune cells infiltrating VAT. We isolated VAT at 16 weeks of HFD feeding from both WT and *Cd300e*$^{-/-}$ mice, followed by single-cell RNA-seq of tissue-resident CD45^{+} immune cells. We applied the Louvain algorithm to identify homogeneous and distinct groups of cells from single-cell RNA-seq data, resulting in the clustering of ~ 23,000 cells into 24 broad immune cell types (Figure 5A; Data S1). We classified the different groups based on expression levels of the most variable genes and used the differentially expressed genes to annotate broad myeloid and lymphoid cell types. Following this approach, we detected considerable differences of the immune cell population in VAT between the two groups of animals (Figure 5B, left panel). The most prominent changes in *Cd300e*$^{-/-}$ mice included an expansion of macrophages, of CD4^{+} and CD8^{+} T cells, in line with above data (Figure 4) and a reduction in B lymphocytes (Figure 5B, right panel). Notably, no differences were observed in blood mononuclear cell composition between WT and *Cd300e*$^{-/-}$ mice, irrespective of the diet regimen (Supplementary Figure 3).

We then sought to functionally characterize the macrophage subset. We identified several differentially expressed genes when comparing WT and *Cd300e*$^{-/-}$ macrophages (Figure 5C, volcano plot). A pathway enrichment analysis revealed significant differences between the two groups after 16 weeks of HFD feeding. In particular, fatty acid metabolism and oxidative phosphorylation pathways were more active in *Cd300e*$^{-/-}$ macrophages, whereas pro-inflammatory responses appeared attenuated (Figure 5D). A more detailed analysis of gene modules uncovered a transcriptional signature enriched for pathways associated with lipid metabolism and phagocytosis. Unexpectedly,

most of these genes were upregulated in *Cd300e*$^{-/-}$ macrophages (Figure 5E). This observation was further validated by real-time PCR analysis on selected genes in F4/80^{+} cells isolated from VAT (Figure 6A).

To corroborate these results with a functional assay, we performed a BODIPY staining on macrophages infiltrating VAT of WT and mutant animals. Our analysis revealed a higher accumulation of neutral lipids within the *Cd300e*$^{-/-}$ cells than their WT counterpart (Figure 6B), further supporting the acquisition of a LAM-like profile by macrophages deficient for CD300e.

Adipocytes from *Cd300e*$^{-/-}$ mice exhibit increased lipogenesis

In adipose tissue containing hypertrophic adipocytes, as typically occurs under conditions of overnutrition, lipids are released by adipocytes, taken up by macrophages, and directed to lysosomes for degradation. However, the accumulation of neutral lipids within *Cd300e*$^{-/-}$ macrophages indicates an excessive lipid burden that exceeds their metabolic handling capacity. Given prior evidence that ATMs regulate lipid flux out of adipose tissue and that increased lipid content in ATMs promotes the production of antilipolytic factors[36], we hypothesized that *Cd300e*$^{-/-}$ macrophages might, through the release of yet unidentified mediators, impair the lipid catabolic capacity of neighbouring adipocytes. Such a mechanism could contribute to the adipocyte hypertrophy observed in knockout mice, by disrupting the local macrophage–adipocyte crosstalk necessary to maintain lipid homeostasis under nutrient-rich conditions.

To test this hypothesis, we isolated adipocytes from the visceral adipose tissue (VAT) of obese animals and examined whether the expression of genes encoding key regulators of lipolysis and lipogenesis was altered in *Cd300e*$^{-/-}$ compared to WT animals. We found that ATGL, the enzyme catalyzing the initial step of triglyceride hydrolysis into FFA and diacylglycerol, was significantly downregulated in adipocytes from *Cd300e*$^{-/-}$ animals relative to WT controls (Figure 7A). Consistent with this, adipocytes from KO mice exhibited a marked upregulation of the lipogenic program, with

increased expression of SREBP-1c, ChREBP, and FAS (Figure 7B). Notably, circulating levels of FFA and TAG were concurrently reduced in the KO mice (Figure 7C-D).

Together, these findings support the hypothesis that *Cd300e*$^{-/-}$ macrophages, by failing to adequately process lipid overload and potentially secreting inhibitory signals, disrupt the homeostatic interplay with adipocytes — thereby promoting adipocyte hypertrophy and contributing to adiposopathy in the context of nutrient excess.

Discussion

ATMs play a central role in lipid handling within adipose tissue, both in health and in obesity. They regulate lipid uptake, storage, and release, contributing to metabolic homeostasis and protecting against lipotoxicity. Lipid uptake by ATMs is largely mediated by scavenger receptors, whose expression is dynamically regulated in both physiological and pathological conditions.

Recent evidence suggests that impaired lysosomal function in ATMs promotes intracellular lipid accumulation, which, in turn, suppresses adipocyte lipolysis via the secretion of anti-lipolytic factors[36]. This has led to the hypothesis that ATMs act as lipid sensors, releasing anabolic signals to alleviate their lipid load.

In this context, CD300e may act as a regulatory sensor that modulates lipid uptake by ATMs, thereby preventing excessive lipid accumulation and limiting the release of anti-lipolytic factors that drive adipocyte hypertrophy. This regulatory role could involve the suppression of genes associated with the signature of LAMs. Supporting this hypothesis, ATMs from CD300e-deficient mice fed a HFD display a pronounced up-regulation of LAM-associated genes and a marked accumulation of neutral lipids compared to their WT counterpart. This is accompanied by a significant upregulation of lipogenic genes and a concomitant downregulation of lipolytic genes in the adipocytes of *Cd300e*$^{-/-}$ mice. The concurrent reduction of FFA and TAG in circulation further reinforces the conclusion that the absence of CD300e promotes excessive lipid retention within adipose tissue, disrupting the macrophage–adipocyte crosstalk necessary to preserve adipose tissue function and restrain the development of adiposopathy.

Neutral lipids in ATMs from *Cd300e*$^{-/-}$ animals are likely to originate from the excess of FFA taken up by these cells during the progression of obesity, esterified and accumulated as TAG, but also from the direct internalization of TAG-rich AdExos.

It is worth highlighting that CD300e has been shown to bind sphingomyelin, a lipid abundant in TAG-rich AdExos. Notably, subjects with obesity exhibit increased release of AdExos compared to lean individuals[37]. Therefore, it is plausible that the up regulation of the immune receptor during obesity

may facilitate efficient uptake of the abundant AdExos, while simultaneously serving as a compensatory mechanism to limit lipid accumulation within ATMs and help preserve adipose tissue homeostasis. In doing so, it may contribute to preventing the progression towards adiposopathy.

The more pronounced accumulation of TAG in the liver of *Cd300e*$^{-/-}$ mice is unlikely to depend on enhanced uptake of circulating FFA, as their levels — consistent with reduced lipolysis in adipose tissue — are lower compared to WT animals, at least under conditions of chronic overnutrition.

One might argue that in the early phases of overnutrition, an initial oversupply of FFA to the liver in *Cd300e*$^{-/-}$ mice could promote TAG synthesis and deposition, and that, at later stages, impaired VLDL secretion could contribute to hepatic steatosis.

Another noteworthy finding from our study is that adipose tissue inflammation does not appear to be a prerequisite for the development of glucose dysmetabolism in the absence of the immune receptor. Although we observed increased macrophage infiltration in the adipose tissue of *Cd300e*$^{-/-}$ mice compared to WT controls, cytokine expression levels remained largely comparable. Despite this, *Cd300e*$^{-/-}$ mice exhibited worsened glucose homeostasis. This observation is consistent with the fact that there is currently minimal evidence indicating that targeting adipose tissue inflammation in humans substantially improves the metabolic syndrome[38].

Taken together, these results suggest that CD300e is crucial for enabling ATMs to acquire a functional LAM phenotype, and that its upregulation in response to overnutrition may serve a protective role by mitigating adipose tissue dysfunction and glucose dysmetabolism in obesity.

RESOURCH AVAILABILITY

Lead contact

Requests for further information and resources should be directed to and will be fulfilled by the lead contact, Marina de Bernard (marina.debernard@unipd.it)

Materials availability

This study did not generate new unique reagents.

Data and code availability

-Any additional information required to reanalyze the data reported in this work is available from the lead contact upon request.

ACKNOWLEDGMENTS

This research was supported by the following funding sources: Ministry of University and Research (PRIN2022 no. 2022YXZ2RB to M.d.B.), PNRR — CN3 National Center for Gene Therapy and Drugs based on RNA Technology (project no. CN0000004) to S.C., and R.V.; PNRR — CN1 National Centre for HPC, Big Data and Quantum Computing" (project no. CN00000013) and CZI EOSS Cycle 6 (project no. EOSS6-0000000644) to G.S; The European Union's Horizon Europe Research and Innovation Programme (project no. 101080329), Horizon 2020 Research and Innovation Programme (project no. 875534) to A.G.

AUTHOR CONTRIBUTIONS

Conceptualization, S.C., M.d.B., A.G., and R.V.; methodology, S.P., S.V., E.T., A.B., S.G., G.S. and F.C.; investigation, S.C., S.P., and S.V.; supervision, S.C. and M.d.B; writing – original draft, M.d.B. and S.C.; writing –review and editing, all authors.

DECLARATION OF INTERESTS

The authors declare no competing interests.

STAR Methods

Patients

In the study patients with obesity were selected according to the following criteria: age 40-70 years with BMI > 30 kg/m^2, while inclusion criteria for enrolled lean healthy controls were age 40-70 years with BMI <25 kg/m^2. Peripheral blood and SAT were collected from lean and obese patients in accordance with the principles of the Helsinki Declaration, and written informed consent was obtained from each patient according to the study protocol approved by the "Comitato Etico Territoriale Area Centro – Est Veneto (CET – ACEV)" (Blood, Protocol number: 2892P; SAT, Protocol number: AOP3650).

Blood samples were collected from 43 obese patients undergoing bariatric surgery and from 35 individuals of normal weight who underwent elective non-oncologic abdominal surgery at the UOSD Chirurgia Bariatrica and UOC Day Surgery/Week Surgery Multidisciplinare of Azienda Ospedale – Università Padova. In addition, SAT was isolated from 3 of these obese during the bariatric surgery and 3 lean patients during the abdominal surgery.

Sample exclusion criteria included chronic substance or alcohol abuse, smoking within the last year leading up to surgery, malignant disorders, uncontrolled thyroid disorders and Cushing's disease. The clinical characteristics of the patients are reported in Supplementary Table 1.

Mice and diet

Wild-type (WT), CD300e constitutive KO (*Cd300e*$^{-/-}$), *Cd300e*$^{fl/fl}$, and *Cd300e*^{LysM} mice from C57BL/6J background were kindly provided by Professor Codolo from University of Padua.

Mice were housed at animal facility of the University of Padova under a 12 h light-dark cycle, with free access to water and to a standard chow diet (4RF25; Mucedola). All experimental procedures were performed on male mice. Starting at age 8 weeks, mice received chow diet as control fat diet (CFD) or 60% lard high-fat diet (HFD; D12492; Sniff Spezialditen GmbH) for 16 weeks. Body weight was recorded weekly. Mice were euthanized at 24 weeks of age by cervical dislocation. All

experiments were conducted under protocol 858/2023-PR, approved by the Italian Ministry of Health and in line with national animal welfare guidelines.

Stromal vascular fraction (SVF) isolation and ATM purification

For human SVF isolation, subcutaneous adipose tissue of 3 obese patients who underwent abdominoplasty and 3 lean control subjects was processed as previously described[39].

For mouse SVF preparation, VAT and SAT fat pads were excised, finely minced, and incubated with 1 mg/ml collagenase type 2 (Gibco) in DMEM/F-12 (Aurogene) containing 10% fetal bovine serum (FBS, Microgem) for 45 min at 37 °C in constant agitation. Cells were filtered through a 100 µm cell strainer and SVF was separated from mature adipocytes by centrifugation at 400*g* for 7 min. Supernatant and adipocyte fraction were removed and SVF was resuspended in DMEM/F-12 2% FBS and filtered through a 70 µm cell strainer. Erythrocytes were lysed in lysis buffer (BD Pharm Lyse; BD Biosciences), washed in DMEM/F-12 2% FBS, and pellet was resuspended in DMEM/F-12 10% FBS for subsequent analysis.

For ATM isolation from SVF of VAT, after filtration through a 70 µm cell strainer, ATMs were isolated with anti-F4/80 Microbeads Ultrapure (Miltenyi Biotec), following the manufacturer's instructions.

Preparation of human SAT stromal vascular fraction conditioned media

Stromal vascular fraction cells were isolated from subcutaneous adipose tissue of 4 patients undergoing plastic surgery and conditioned media were prepared as reported previously[40]. Briefly, cell suspension was seeded in DMEM/F12 supplemented with 10% FBS (5×10^5 cells/well in 24-well plates). After 24 h, cells were washed twice with sterile PBS (Microgem) and the medium was replaced with low-glucose DMEM (Gibco) phenol red and FBS free. After 24 h, conditioned medium was collected (SAT-CM) and instantly frozen in liquid nitrogen.

Human peripheral blood monocyte isolation and treatment

Monocytes were purified from buffy coats of healthy donors by density gradient protocol, as described previously[41].

To evaluate the effect of conditioned media obtained from stromal vascular fraction of SAT on CD300e expression, monocytes were plated at a density of 1.2×10^6 per well in 24-well in 500 µL of RPMI (Gibco) 10% FBS, 4 mM Hepes (Corning), 50 µg/mL of gentamycin (Gibco), 50% SAT-CM. After 24 h, cells were processed for subsequent analyses.

Metabolic tolerance tests

One week before the conclusion of HFD protocol, glucose tolerance test (GTT) and insulin tolerance test (ITT) were conducted to determine HFD-induced alterations in glucose homeostasis and insulin sensitivity. For GTT, following an overnight fasting, mice underwent i.p. injection of glucose (2 g/kg, Mallinckrodt Baker, Inc.). For ITT, following a 5-h fasting, insulin (0.75 U/kg, Insuman Rapid, Sanofi) was injected i.p. Glycemia was measured immediately before and at 15, 30, 60, 90, and 120 min after glucose or insulin administration. Glucose level was determined from tail blood using Accu-Chek Guide glucometer (Roche Diabetes Care).

Tissue and blood collection from mice

Blood was collected by mandibular vein puncture immediately before sacrifice in EDTA-treated tubes. For plasma preparation, blood was centrifuged at 2,000g for 15 min at RT and the plasma transferred in a separate tube. After separation, plasma was stored at -80 °C for further analysis.

SAT, VAT, and liver were harvested and weighted. After rinsing in PBS, tissues were divided into small pieces (0.5 cm^3). Pieces dedicated to RNA extraction or to lipidomic analysis were kept at -80 °C, while pieces intended for histological analysis were fixed in a 4% paraformaldehyde solution (BioOptica) in PBS for 24 h and then embedded in paraffin (BioOptica); tissues that were meant to

stromal vascular fraction isolation and subsequent procedure were used immediately after the dissection.

Tissue staining

Hematoxylin and eosin (H&E) staining was performed on 2-micron-thick formalin-fixed, paraffin-embedded VAT, SAT, and liver tissue sections. Bright field images were acquired with the DM6 microscope (Leica) using LasX software. VAT and SAT images were analyzed with Fiji (ImageJ) software to determine the area of adipocytes.

Quantification of triglycerides and FFA

Hepatic triglycerides and plasma FFA were measured using specific commercial kits, according to the manufacturers' instructions. Hepatic triglyceride content was quantified using the Triglyceride Assay Kit (Abcam). Plasma levels of FFA were determined with the FFA Assay kit (Abbexa).

Lipid composition

Lipidomic analyses were performed in plasma and liver tissues using liquid chromatography/quadrupole time-of-flight mass spectrometry (UHPLC -QTOF, 1290 Infinity-6545 Agilent Technology, Santa Clara, CA) in positive ion ionization equipped with an Agilent ZORBAX Eclipse Plus C18 2.1 × 100 mm 1.8-Micron column at 50°C. TAG were quantified using internal standard added to each sample, specifically TAG(15:0/15:0/15:0) (purchased from Avanti Polar Lipids, Alabaster, AL, and Larodan, Solna, SE).

About 25 mg of liver tissues were homogenized using Precellys Evolution Homogenizer (Bertin Instruments, Frankfurt, Germany) (3 cycles of 30 sec at 5800 rpm, with 20 sec pause between each cycle, at 4°C) and samples were centrifuged for 20 min at 12,900 rpm at 4°C to remove proteins from samples. Lipid species were extracted with modified Folch method using 900 µl of chloroform:methanol (2:1) and 200 µl of water, centrifuged for 15 min at 12,900 rpm at 4°C and

down phases were dry under gentle nitrogen flux and resuspended in 200 µl of chloroform:methanol (1:1) solution. For plasma lipidomic analysis, 10 µl of samples were deproteinized with 150 µl of cold methanol (Sigma-Aldrich) and 10µl of internal standard and centrifuged at 12,900 rpm at 4°C for 20 min.

Flow Cytometry

Human subcutaneous SVF

SAT stromal vascular fraction was obtained as detailed above. Cells were resuspended in FACS buffer (PBS, 2% FBS) and incubated for 15 min at RT with Human TruStain FcX (Biolegend) to block Fc receptors. 0.5 x 10^6 cells were stained with the unconjugated monoclonal antibody anti-CD300e (clone UPH2, ThermoFisher) followed by a goat anti-mouse Alexa Fluor 647 antibody (ThermoFisher), PE-Cy7-conjugated anti-CD45 (clone HI30, BD Biosciences) and BV785-conjugated anti-CD11b (clone M1/70, Biolegend). Zombie Aqua Fixable Viability Dye (Biolegend) was used to exclude dead cells. Cells were fixed with 3.6% formaldehyde and permeabilized with PermWash solution (1% FBS, 0.2% saponin in PBS). Cells were stained with PE-conjugated anti-CD68 monoclonal antibody (clone Y1/82A; eBioscience), resuspended in FACS buffer, and acquired by LSR Fortessa X-20 Cell Analyzer (BD Biosciences). Data were analysed using FlowJo software, version 10.3 (Tree Star Inc., Ashland, OR, USA).

Human peripheral blood monocytes

150 µL of peripheral blood collected into EDTA-treated tubes were incubated for 5 min at RT with 3 mL of lysis buffer (BD Pharm Lyse, BD Biosciences) to lyse erythrocytes. Cells were washed with FACS buffer (PBS, 2% FBS) and incubated with Human TruStain FcX (Biolegend) for 15 min at RT to block Fc receptors. At the end of incubation cells were stained with the following monoclonal antibodies: PE-conjugated anti-CD300e (clone UP-H2, Biolegend), APC-conjugated anti-HLA-DR (clone L243, Biolegend), FITC-conjugated anti-CD3 (clone UCHT1, Biolegend), FITC-conjugated-CD19 (clone HIB19, eBioscience) and FITC-conjugated-CD56 (clone TULY56, eBioscience),

PerCP/Cyanine5.5-conjugated anti-CD14 (clone 63D3, Biolegend) and BV785-conjugated anti-CD16 (clone 3G8, Biolegend). The BD Horizon™ fixable viability stain 780 (BD Biosciences) was used to exclude dead cells from the analysis. Cells were resuspended in FACS buffer and analysed by LSR Fortessa X-20 Cell Analyzer (BD Biosciences). The gating strategy adopted to analyse monocytes subsets was previously reported[42] and illustrated in Supplementary Figure 4. Data were analysed using FlowJo software, version 10.3 (Tree Star Inc., Ashland, OR, USA).

Human monocytes treated with SAT-CM

Purified cells were harvested from culture plates using 5 mM Na-EDTA (AppliChem) in PBS, pH 7.5 and incubated for 15 min at RT with Human TruStain FcX (Biolegend) to block Fc receptors. Cells were stained for 15 min at RT with the monoclonal antibody PE-conjugated anti-CD300e (clone UPH2, Biolegend). The BD Horizon™ fixable viability stain 780 (BD Biosciences) was used to exclude dead cells from the analysis. Cells were washed, resuspended in FACS buffer and analysed by LSR Fortessa X-20 Cell Analyzer (BD Biosciences). Data were analysed using FlowJo software, version 10.3 (Tree Star Inc., Ashland, OR, USA).

Mouse subcutaneous and visceral SVF

0.5 x 10^6 cells isolated from SAT and VAT stromal vascular fraction, as described above, were incubated with TruStain FcX PLUS (BioLegend) for 10 min at 4°C to block Fc receptors. Depending on the experiment, cells were stained with combinations of the following antibodies: PE-Cy7-conjugated anti-CD45 (clone 30-F11, Biolegend), BV785-conjugated anti-CD11b (clone M1/70, Biolegend), BV421-conjugated anti-F4/80 (clone BM8, Biolegend), PE-conjugated anti-TREM2 (clone 6E9, Biolegend), APC-conjugated anti-CD36 (clone HM36, Biolegend), BV650-conjugated anti-CD4 (clone RM4-5, Biolegend), AlexaFluor700-conjugated anti-mouse CD8a (clone QA17A07, Biolegend).

The BD Horizon™ fixable viability stain 780 (BD Biosciences) or Zombie Aqua Fixable Viability Dye (Biolegend) were used to exclude dead cells from the analysis. Cells were resuspended in FACS

buffer and analysed by LSR Fortessa X-20 Cell Analyzer (BD Biosciences). Data were analysed using FlowJo software, version 10.3 (Tree Star Inc., Ashland, OR, USA).

Mouse peripheral blood

Peripheral blood was transferred in a round-bottom tube and incubated with lysis buffer (BD Pharm Lyse; BD Biosciences) to lyse erythrocytes. Cells were incubated for 10 min at 4 °C with TruStain FcX PLUS (BioLegend) and stained with the monoclonal antibodies FITC-conjugated anti-CD45 (clone 30-F11; BioLegend), PE-conjugated anti-CD19 (clone 1D3/CD19; BioLegend), PE-Cy7-conjugated anti-Ly6G (clone 1A8; BioLegend), PerCP/Cyanine5.5-conjugated anti-CD8a (clone 53-6.7; BioLegend), APC-conjugated anti-CD4 (clone RM4-5; BioLegend), APC-Cy7-conjugated anti-CD3e (clone 145-2C11; BioLegend), BV421-conjugated anti-Ly6C (clone HK1.4; BioLegend), and BV785-conjugated anti-CD11b (clone M1/70; BioLegend). Zombie Aqua Fixable Viability Dye (Biolegend) was used to exclude dead cells. Cells were resuspended in FACS buffer and analyzed by LSR Fortessa X-20 Cell Analyzer (BD Biosciences). Data were analysed using FlowJo software, version 10.3 (Tree Star Inc., Ashland, OR, USA).

RNA extraction and qRT-PCR

Snap-frozen tissue pieces were disrupted in TRIzol reagent (Thermo Fisher Scientific) using TissueLyser II (QIAGEN), while cell pellets were resuspended in TRIzol and disaggregated by pipetting, and RNA was extracted following manufacturer instructions. After quantification using NanoDrop Lite Spectrophotometer (Thermo Scientific), 1 µg of RNA was retrotranscribed using the High-Capacity cDNA Reverse Transcription Kit (Thermo Fisher Scientific) and the retrotranscription reaction conditions recommended by the manufacturer. 5 ng of cDNA were used in qRT-PCR reaction performed in QuantStudio™ 5 Real-Time PCR System (Applied Biosystems); the reaction was performed using PowerUp™ SYBR™ Green Master Mix for qPCR (Applied Biosystems). For human samples, data were normalized to the endogenous reference gene β-actin; for mouse samples,

data were normalized to the endogenous reference gene 18S and confirmed using a different reference gene (β-actin; data not shown). Primer sequences are reported in Supplementary Table 2.

Single-cell labelling with BD® Mouse Immune Single-Cell Multiplexing Kit and sorting of CD45$^+$ cells

For single-cell transcriptome analysis, 200,000 VAT-SVF cells from 3 WT and 3 *Cd300e*$^{-/-}$ mice were washed and incubated for 20 min with 20 µL of sample-tag (BD Biosciences) linked to MHC class I. After 3 washing steps, cells from all 6 animals were pooled in a single tube and stained with PE/Cyanine7 anti-mouse CD45 (BioLegend) and BD Horizon™ Fixable Viability Stain 780 (BD Biosciences); 125,000 live CD45$^+$ cells were collected after cell sorting with FACS Aria III (BD Biosciences).

Single cell capture and cDNA library preparation with BD Rhapsody™ System

Single cell synthesis of cDNA was performed strictly in accordance with manufacturer's instructions. Briefly, cells were stained with Calcein AM (Thermo Fisher Scientific) and DRAQ7™ (BD Pharmingen) to assess cell viability and determine cell concentration using the BD Rhapsody Scanner (BD Biosciences). 60,000 cells were loaded onto the primed BD Rhapsody™ Cartridge (BD Biosciences) that was then transferred to the BD Rhapsody™ Express Instrument (BD Biosciences). BD Rhapsody™ Enhanced Cell Capture Beads were loaded to the cartridge to allow single cell capture in the microwells of the cartridge and a final washing step to remove the excessive beads. After cell lysis within the microwells, beads were retrieved before reverse transcription. mRNA whole transcriptome approach (WTA) was applied for priming, extension, and amplification of the transcripts. Sample tag libraries and cDNA libraries were generated separately after final addition of indexes through PCR. Library concentrations were optimal at 3.04 ng/µL (Sample Tag) and 13.8 ng/µL (WTA), measured with Qubit4 fluorometer (Invitrogen). TapeStation analysis (Agilent) confirmed expected peak sizes of 262 bp and 396 bp, respectively.

Sequencing, statistical and single-cell data analyses

Libraries were sequenced on the NovaSeq 6000 platform (Illumina) using a 2 × 150 bp paired-end read configuration, generating a total of 3,468 million reads. Overall, 92.4% of the reads contained a valid cell label and an UMI that aligned uniquely. Initial estimates indicated 29,230 putative sampled cells. Gene expression profiles were quantified using the BD Rhapsody Sequence Analysis Pipeline (v2.2) with the RhapRef_Mouse_WTA_2023-02 reference annotation. To mitigate the impact of doublet artifacts, scDblFinder (v1.18.0) was employed to remove likely doublets, filtering out approximately 7% of cells. Further quality control was performed to exclude cells with high mitochondrial RNA content (≥15%), indicative of cell lysis. Cells were filtered to include only those expressing at least 1000 genes and having between 1,000 and 50,000 associated reads. The final dataset consisted of 22,959 cells for downstream analysis. Gene expression data were processed with the R package Seurat (v5.1.0). Gene counts were normalized using the SCTransform algorithm[43], which models technical effects to stabilize variance and remove technical confounders. Clustering was performed using the Louvain algorithm to automatically identify cell subpopulations based on distinct gene expression profiles. We adopted a 0.5 resolution level to balance clustering granularity and biological interpretability. Cell type identities were automatically inferred using the Azimuth package (v0.5.0), and the resulting annotation was manually refined to identify broad myeloid and lymphoid cell types based on marker gene profiles. Differential gene expression analysis was computed using the pseudo bulk approach implemented by the Libra package (v1.0.0-1, edgeR method[44]). We applied a false discovery rate (FDR) threshold of 0.05 to identify significantly altered gene expression profiles.

References

1. Choe, S. S., Huh, J. Y., Hwang, I. J., Kim, J. I. & Kim, J. B. Adipose Tissue Remodeling: Its Role in Energy Metabolism and Metabolic Disorders. *Front. Endocrinol.* **7**, (2016).
2. Vegiopoulos, A., Rohm, M. & Herzig, S. Adipose tissue: between the extremes. *EMBO J.* **36**, 1999–2017 (2017).
3. Kahn, C. R., Wang, G. & Lee, K. Y. Altered adipose tissue and adipocyte function in the pathogenesis of metabolic syndrome. *J. Clin. Invest.* **129**, 3990–4000 (2019).
4. Favaretto, F., Bettini, S., Busetto, L., Milan, G. & Vettor, R. Adipogenic progenitors in different organs: Pathophysiological implications. *Rev. Endocr. Metab. Disord.* **23**, 71–85 (2022).
5. Hoffmann, J., Romey, R., Fink, C. & Roeder, T. Drosophila as a Model to Study Metabolic Disorders. in *Yellow Biotechnology I* (ed. Vilcinskas, A.) vol. 135 41–61 (Springer Berlin Heidelberg, Berlin, Heidelberg, 2013).
6. Cai, Z., Huang, Y. & He, B. New Insights into Adipose Tissue Macrophages in Obesity and Insulin Resistance. *Cells* **11**, 1424 (2022).
7. Nance, S. A., Muir, L. & Lumeng, C. Adipose tissue macrophages: Regulators of adipose tissue immunometabolism during obesity. *Mol. Metab.* **66**, 101642 (2022).
8. Emont, M. P. *et al.* A single-cell atlas of human and mouse white adipose tissue. *Nature* **603**, 926–933 (2022).
9. Vijay, J. *et al.* Single-cell analysis of human adipose tissue identifies depot- and disease-specific cell types. *Nat. Metab.* **2**, 97–109 (2020).
10. Jaitin, D. A. *et al.* Lipid-Associated Macrophages Control Metabolic Homeostasis in a Trem2-Dependent Manner. *Cell* **178**, 686-698.e14 (2019).
11. Chavakis, T., Alexaki, V. I. & Ferrante, A. W. Macrophage function in adipose tissue homeostasis and metabolic inflammation. *Nat. Immunol.* **24**, 757–766 (2023).
12. Zechner, R., Kienesberger, P. C., Haemmerle, G., Zimmermann, R. & Lass, A. Adipose triglyceride lipase and the lipolytic catabolism of cellular fat stores. *J. Lipid Res.* **50**, 3–21 (2009).
13. Deng, L., Kersten, S. & Stienstra, R. Triacylglycerol uptake and handling by macrophages: From fatty acids to lipoproteins. *Prog. Lipid Res.* **92**, 101250 (2023).
14. Flaherty, S. E. *et al.* A lipase-independent pathway of lipid release and immune modulation by adipocytes. *Science* **363**, 989–993 (2019).
15. Raposo, G. & Stoorvogel, W. Extracellular vesicles: Exosomes, microvesicles, and friends. *J. Cell Biol.* **200**, 373–383 (2013).
16. Crewe, C. *et al.* An Endothelial-to-Adipocyte Extracellular Vesicle Axis Governed by Metabolic State. *Cell* **175**, 695-708.e13 (2018).
17. Silverstein, R. L. & Febbraio, M. CD36, a Scavenger Receptor Involved in Immunity, Metabolism, Angiogenesis, and Behavior. *Sci. Signal.* **2**, (2009).
18. Chen, Y., Zhang, J., Cui, W. & Silverstein, R. L. CD36, a signaling receptor and fatty acid transporter that regulates immune cell metabolism and fate. *J. Exp. Med.* **219**, e20211314 (2022).
19. Fabris, R. *et al.* Preferential Channeling of Energy Fuels Toward Fat Rather Than Muscle During High Free Fatty Acid Availability in Rats. *Diabetes* **50**, 601–608 (2001).
20. Nisoli, E. *et al.* Induction of fatty acid translocase/CD36, peroxisome proliferator-activated receptor-gamma2, leptin, uncoupling proteins 2 and 3, and tumor necrosis factor-alpha gene expression in human subcutaneous fat by lipid infusion. *Diabetes* **49**, 319–324 (2000).
21. Borrego, F. The CD300 molecules: an emerging family of regulators of the immune system. *Blood* **121**, 1951–1960 (2013).
22. Isobe, M. *et al.* The CD300e molecule in mice is an immune-activating receptor. *J. Biol. Chem.* **293**, 3793–3805 (2018).
23. Simhadri, V. R. *et al.* Human CD300a binds to phosphatidylethanolamine and phosphatidylserine, and modulates the phagocytosis of dead cells. *Blood* **119**, 2799–2809 (2012).
24. Coletta, S. *et al.* The antigen CD300e drives T cell inflammation in adipose tissue and elicits

an antibody response predictive of the insulin sensitivity recovery in obese patients. *J. Inflamm.* **19**, 21 (2022).
25. van der Kolk, B. W. *et al.* Differential Mitochondrial Gene Expression in Adipose Tissue Following Weight Loss Induced by Diet or Bariatric Surgery. *J. Clin. Endocrinol. Metab.* **106**, 1312–1324 (2021).
26. Van Der Kolk, B. W. *et al.* Molecular pathways behind acquired obesity: Adipose tissue and skeletal muscle multiomics in monozygotic twin pairs discordant for BMI. *Cell Rep. Med.* **2**, 100226 (2021).
27. Weisberg, S. P. *et al.* Obesity is associated with macrophage accumulation in adipose tissue. https://www.jci.org/articles/view/19246/pdf (2003) doi:10.1172/JCI19246.
28. Weisberg, S. P. *et al.* CCR2 modulates inflammatory and metabolic effects of high-fat feeding. *J. Clin. Invest.* **116**, 115–124 (2006).
29. Kanda, H. MCP-1 contributes to macrophage infiltration into adipose tissue, insulin resistance, and hepatic steatosis in obesity. *J. Clin. Invest.* **116**, 1494–1505 (2006).
30. Zenarruzabeitia, O. *et al.* The expression and function of human CD300 receptors on blood circulating mononuclear cells are distinct in neonates and adults. *Sci. Rep.* **6**, 32693 (2016).
31. Barizza, A. *et al.* CD300e as a Driver of Immunosuppressive Tumor Microenvironment in Colorectal Cancer. Preprint at https://doi.org/10.1101/2024.09.01.610700 (2024).
32. Marjot, T., Moolla, A., Cobbold, J. F., Hodson, L. & Tomlinson, J. W. Nonalcoholic Fatty Liver Disease in Adults: Current Concepts in Etiology, Outcomes, and Management. *Endocr. Rev.* **41**, 66–117 (2020).
33. Brckalo, T. *et al.* Functional analysis of the CD300e receptor in human monocytes and myeloid dendritic cells. *Eur. J. Immunol.* **40**, 722–732 (2010).
34. Chait, A. & Den Hartigh, L. J. Adipose Tissue Distribution, Inflammation and Its Metabolic Consequences, Including Diabetes and Cardiovascular Disease. *Front. Cardiovasc. Med.* **7**, 22 (2020).
35. Gao, F., Litchfield, B. & Wu, H. Adipose tissue lymphocytes and obesity. *J. Cardiovasc. Aging* **4**, 5 (2024).
36. Xu, X. *et al.* Obesity Activates a Program of Lysosomal-Dependent Lipid Metabolism in Adipose Tissue Macrophages Independently of Classic Activation. *Cell Metab.* **18**, 816–830 (2013).
37. Matilainen, J. *et al.* Increased secretion of adipocyte-derived extracellular vesicles is associated with adipose tissue inflammation and the mobilization of excess lipid in human obesity. *J. Transl. Med.* **22**, 623 (2024).
38. Kusminski, C. M., Bickel, P. E. & Scherer, P. E. Targeting adipose tissue in the treatment of obesity-associated diabetes. *Nat. Rev. Drug Discov.* **15**, 639–660 (2016).
39. Coletta, S. *et al.* The immune receptor CD300e negatively regulates T cell activation by impairing the STAT1-dependent antigen presentation. *Sci. Rep.* **10**, 16501 (2020).
40. De Mario, A. *et al.* Mitochondrial Ca2+ signaling is a hallmark of specific adipose tissue-cancer crosstalk. *Sci. Rep.* **14**, 8469 (2024).
41. D'Elios, M. M. *et al.* The Helicobacter cinaedi antigen CAIP participates in atherosclerotic inflammation by promoting the differentiation of macrophages in foam cells. *Sci. Rep.* **7**, 40515 (2017).
42. Marimuthu, R. *et al.* Characterization of Human Monocyte Subsets by Whole Blood Flow Cytometry Analysis. *J. Vis. Exp. JoVE* e57941 (2018) doi:10.3791/57941.
43. Hafemeister, C. & Satija, R. Normalization and variance stabilization of single-cell RNA-seq data using regularized negative binomial regression. *Genome Biol.* **20**, 296 (2019).
44. Squair, J. W. *et al.* Confronting false discoveries in single-cell differential expression. *Nat. Commun.* **12**, 5692 (2021).

Figure Legends

Figure 1

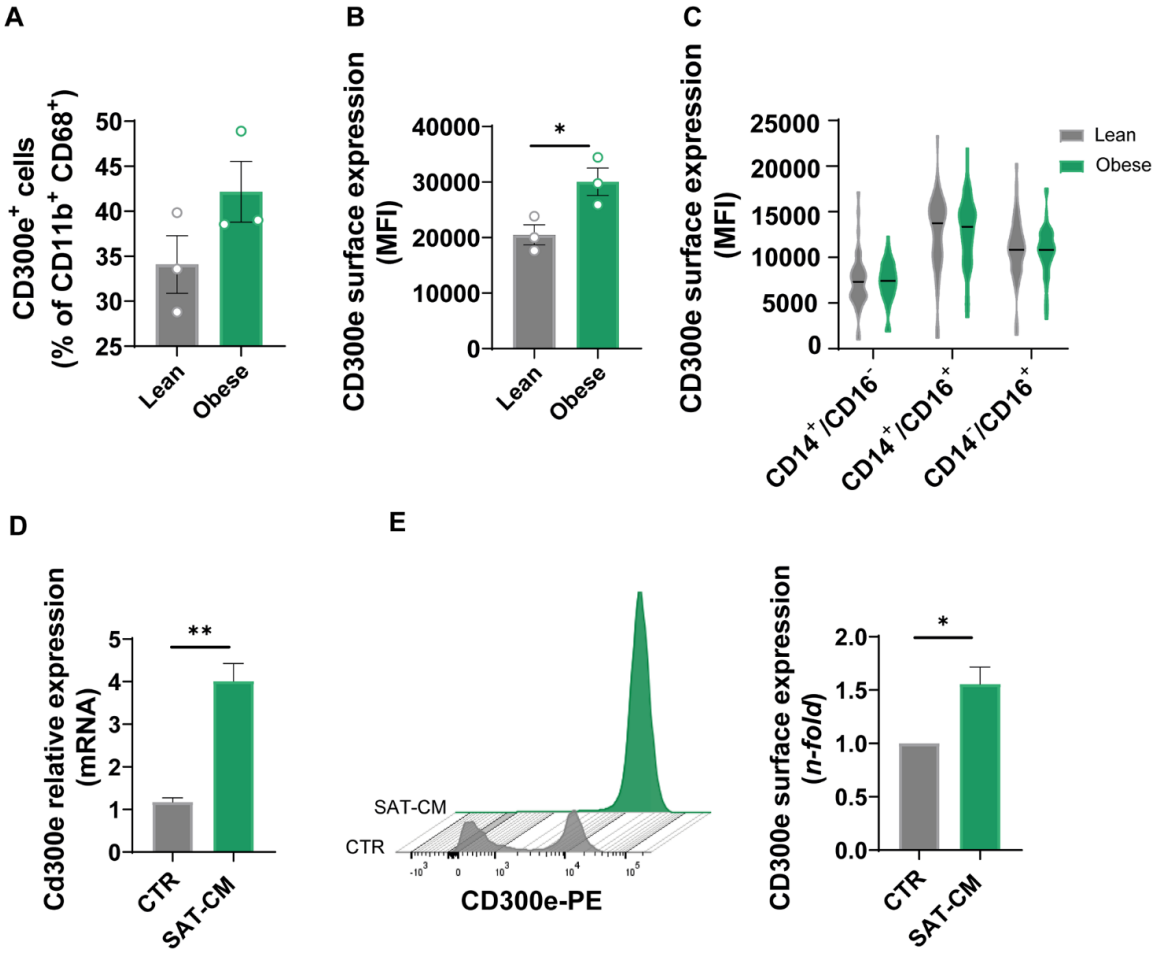

Figure 1. Local upregulation of CD300e in adipose tissue macrophages in obesity. A) Flow cytometry analysis of CD300e$^+$ cells, gated on macrophages (CD11b$^+$CD68$^+$), in SVF from SAT of lean and obese subjects. Data are shown as mean ± SEM (n=3). **B)** Surface expression of CD300e on macrophages (CD11b$^+$CD68$^+$ cells) infiltrating SVF of lean and obese SAT. Data are expressed as mean fluorescence intensity (MFI) ± SEM (n=3). **C)** Violin plot of surface expression of CD300e on peripheral blood circulating monocytes of lean and obese SAT. Circulating monocytes have been identified as classical (CD14$^+$CD16$^-$), intermediate (CD14$^+$CD16$^+$) and non-classical (CD14$^-$CD16$^+$). (lean, n=35; obese, n=43). **D)** Expression of CD300e mRNA on freshly isolated monocytes cultured for 24 h with conditioned medium derived from the SVF of obese SAT (SAT-CM). Data were normalized on β-actin as endogenous reference genes and are expressed as $2^{-\Delta\Delta Ct}$ relative to untreated monocytes (CTR). Data are expressed as mean ± SEM (SAT donors, n=4). **E) left panel:** representative histograms of CD300e surface expression in monocytes stimulated as in **D)**. Untreated and treated monocytes are show in grey and green, respectively. **Right panel:** median fluorescence intensity (MFI) of CD300e ± SEM of 4 independent experiments. Expression levels of CD300e are expressed as *n*-fold change relative to untreated monocytes set as 1. Significance was determined by Student's t-test. *$p<0.05$; **, $p< 0.01$.

Figure 2

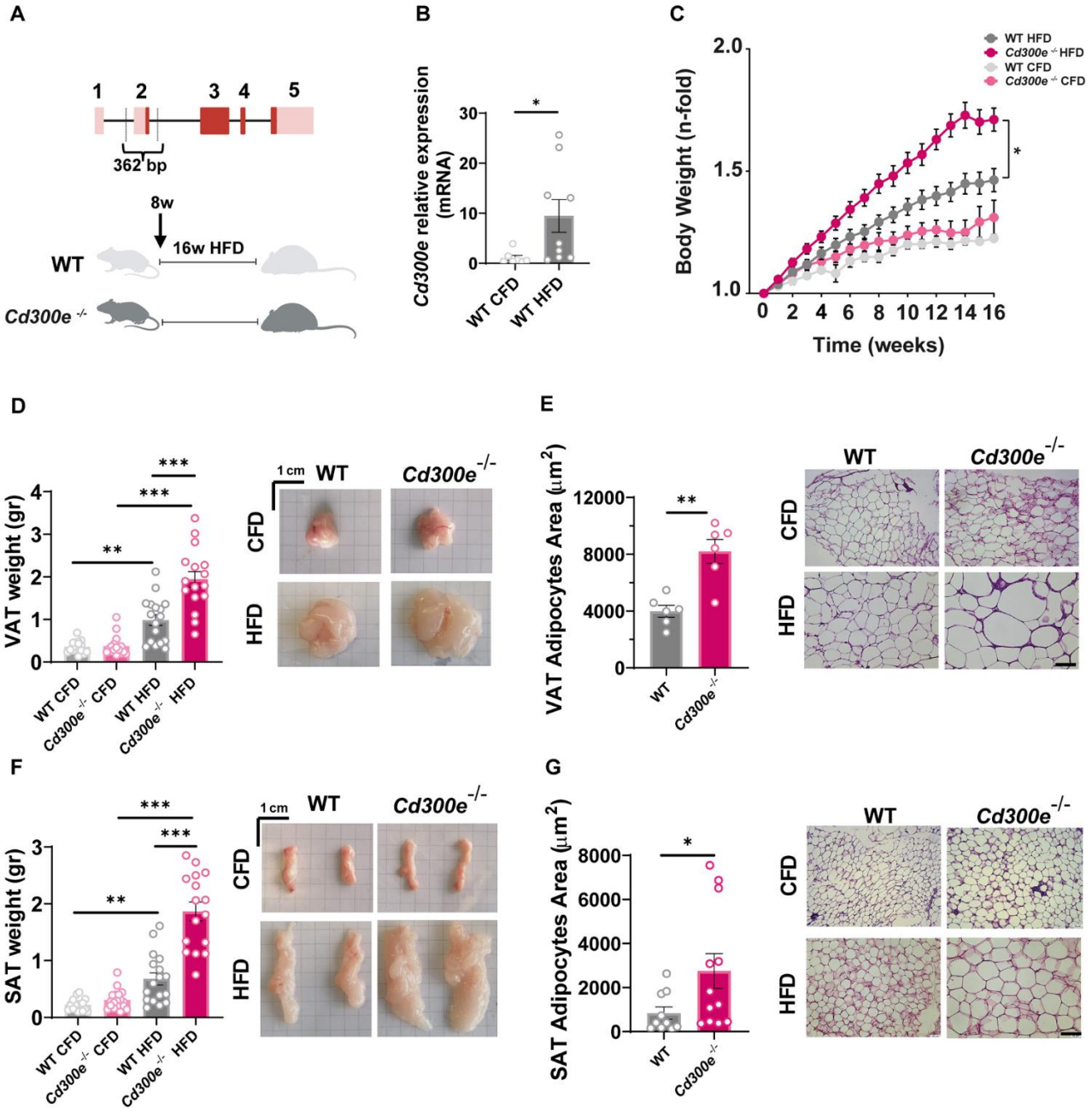

Figure 2. CD300e prevents the adipocyte hypertrophy induced by excessive energy intake. A) Upper panel: Representation of mouse *Cd300e* gene with introns (black line) and exons (red boxes); the latter include untranslated (UTR) regions (light red) and protein-coding regions (dark red). *Cd300e*$^{-/-}$ mice carry a deletion of 362 bp encompassing exon 2, together with upstream and downstream intronic regions. Lower panel: Schematic representation of diet-induced obesity model. **B**) Expression of *Cd300e* mRNA was evaluated in VAT of WT mice after 16 weeks of control diet (CFD) or high fat diet (HFD). mRNA expression was determined by qRT-PCR and data were normalized to an endogenous reference gene (18S). Expression levels of HFD mice are relative to

chow diet-fed mice. Data are shown as mean ± SEM (CFD, n=7; HFD, n=9). **C**) Body weight of WT and *Cd300e*$^{-/-}$ mice under CFD or HFD feeding. Data are shown as mean ± SEM (CFD, n=10; HFD, n=22). Significance was determined by one-way ANOVA test. *, $p < 0.05$). **D**) VAT mass of WT and KO mice after 16 weeks of CFD or HFD feeding; data are shown as mean ± SEM (n=16/group). Significance was determined by one-way ANOVA test. **, $p < 0.01$; ***, $p<0.001$. Representative images of gross morphology of VAT from mice of the indicated genotype are reported. **E**) Cross sectional area of VAT adipocytes of WT and *Cd300e*$^{-/-}$ mice after 16 weeks of HFD feeding (n=286 adipocytes from WT mice; n=280 adipocytes from *Cd300e*$^{-/-}$ mice; adipocytes derived from 6 mice/genotype). Significance was determined by Student's t-test. **, $p < 0.01$. Sections of VAT from WT and *Cd300e*$^{-/-}$ mice after CFD or HFD feeding were generated and stained with H&E. Scale bar = 100 µm. **F**) SAT mass of WT and *Cd300e*$^{-/-}$ mice after 16 weeks of CFD or HFD feeding, data are shown as mean ± SEM (n=16/group). Significance was determined by one-way ANOVA test. **, $p < 0.01$; ***, $p<0.001$. Representative images of gross morphology of SAT from mice of the indicated genotype are reported. **G**) Cross sectional area of SAT adipocytes of WT and *Cd300e*$^{-/-}$ mice after 16 weeks of HFD feeding (n=917 adipocytes from WT mice; n=750 adipocytes from *Cd300e*$^{-/-}$ mice; adipocytes derived from 10 WT mice and 12 *Cd300e*$^{-/-}$ mice). Significance was determined by Student's t-test. *, $p < 0.05$. Sections of SAT from WT and *Cd300e*$^{-/-}$ mice after CFD or HFD feeding were generated and stained with H&E. Scale bar = 100 µm.

Figure 3

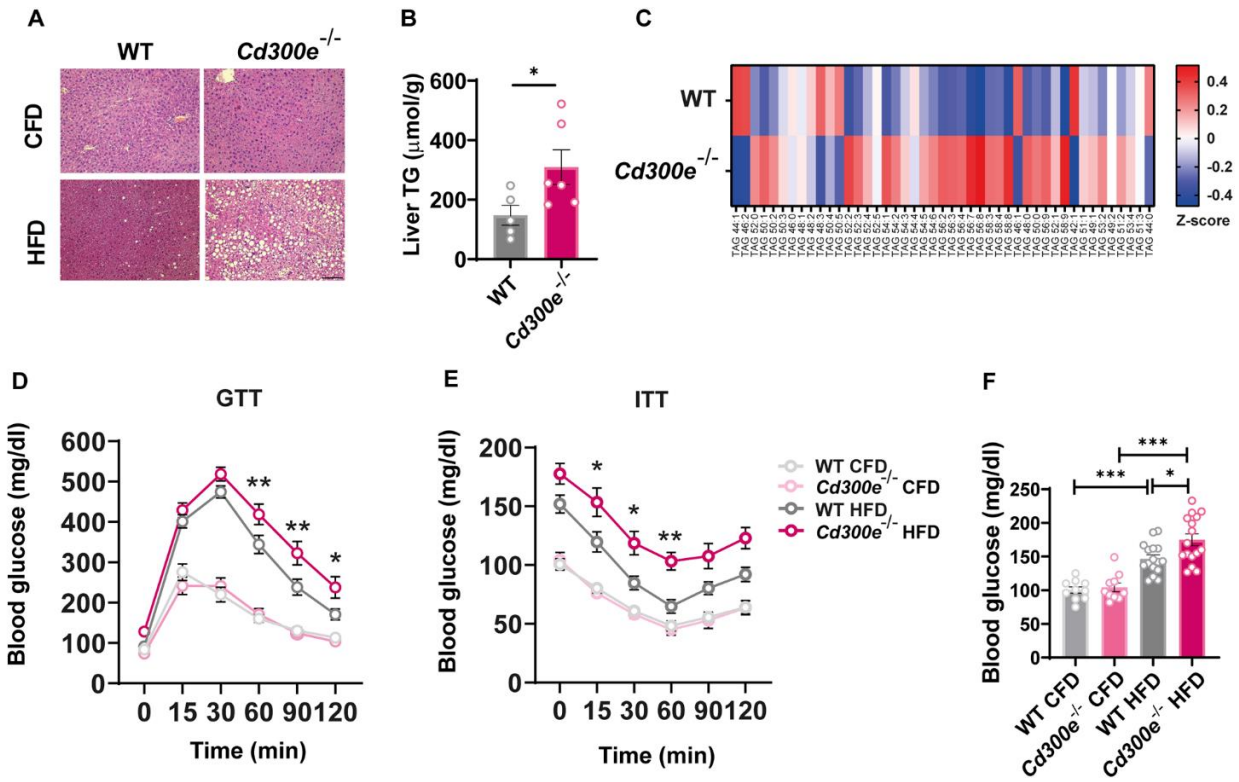

Figure 3. CD300e prevents liver steatosis and glucose dysmetabolism. A) Sections of liver from WT and *Cd300e*$^{-/-}$ mice after 16 weeks of CFD or HFD were generated and stained with H&E. Scale bar = 100 µm. **B**) Biochemical quantification of intrahepatic triglycerides (TAG) in liver of WT and *Cd300e*$^{-/-}$ mice after 16 weeks of HFD feeding. Data are shown as mean ± SEM (n=6/genotype). Significance was determined by Student's t-test. *, $p < 0.05$. **C**) Heat map visualizing phenotypes of

TAG lipidomes detected in liver of WT and *Cd300e*$^{-/-}$ mice after 16 weeks of HFD feeding. Data are expressed as mean of pmol/mg z-score (n=12/genotype). **D-E**) GTT and ITT of WT and *Cd300e*$^{-/-}$ mice after 16 weeks of CFD and HFD. Data are shown as mean ± SEM (CFD, n=12; HFD, n=16). Significance was determined by two-way ANOVA test. *, $p< 0.05$; **, $p< 0.01$. **F**) Basal levels of glucose were measured in blood of 5-h-fasted WT and *Cd300e*$^{-/-}$ mice at the end of the diet regimen. Data are shown as mean ± SEM (CFD, n=10; HFD, n=16). Significance was determined by one-way ANOVA test. *, $p< 0.05$; ***, $p<0,001$.

Figure 4

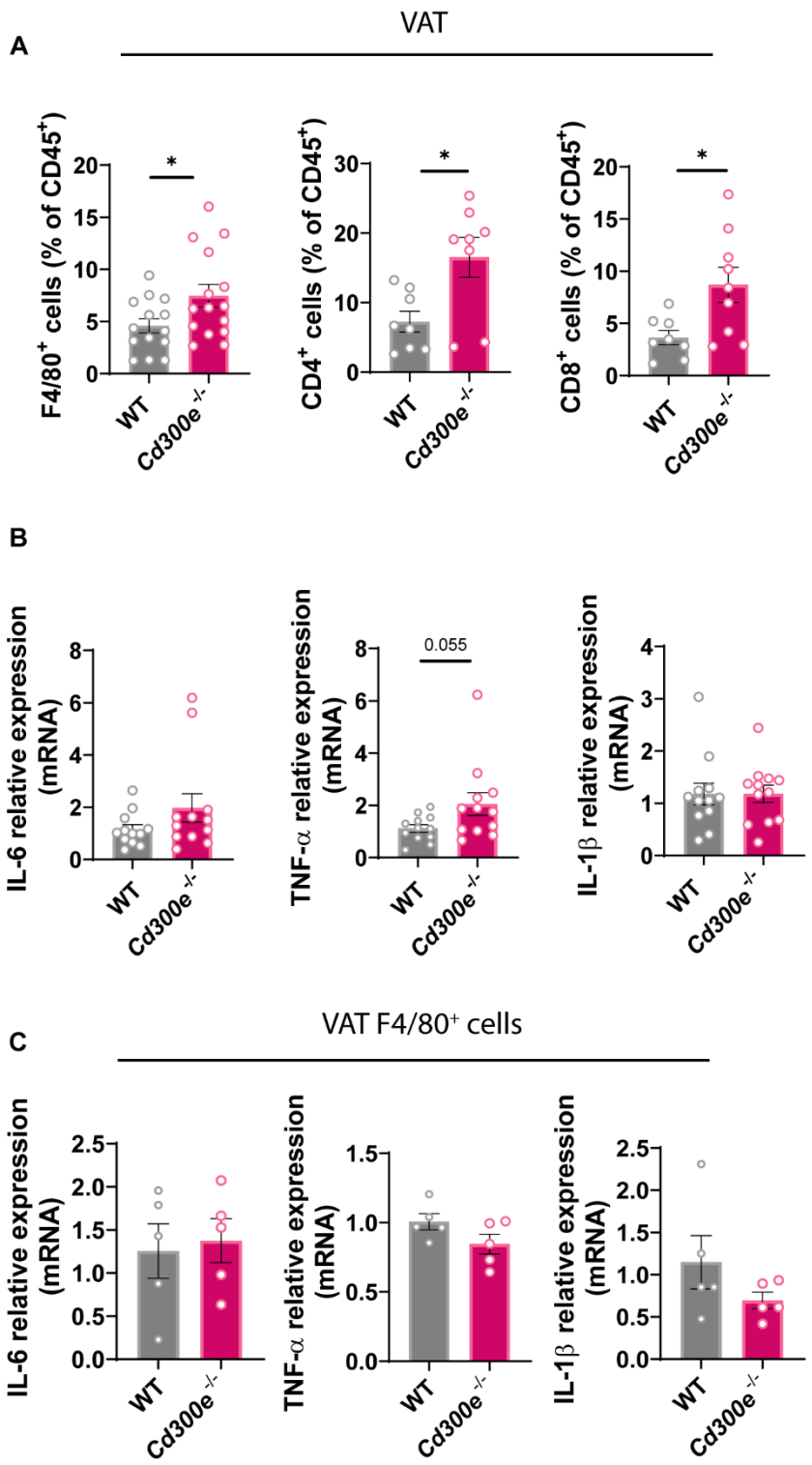

Figure 4. *Cd300e*$^{-/-}$ mice lack significant AT inflammation. A) F4/80^{+} cells, CD4^{+} and CD8^{+} T lymphocytes (gated on CD45^{+} cells) were analyzed by flow cytometry in VAT infiltrates from WT and *Cd300e*$^{-/-}$ mice after 16 weeks of chow or HFD feeding. Data are shown as mean ± SEM (F4/80^{+} cells, n=15; CD4^{+} and CD8^{+} T cells, n=8). Significance was determined by Student's t test. *, $p < 0.05$. **B-C)** mRNA expression of IL-6, TNF-α and IL-1β was evaluated by qRT-PCR on VAT and on F4/80^{+} cells isolated from VAT of WT and *Cd300e*$^{-/-}$ mice after 16 weeks of HFD feeding. Data were

normalized on 18S as endogenous reference genes and are expressed as $2^{-\Delta\Delta Ct}$ relative to WT mice. Data are expressed as mean ± SEM (VAT, n=12/genotype; F4/80^{+}, n=5/genotype). Statistical significance was determined by Student's t test. P-values near the threshold for statistical significance are reported in the figure.

Figure 5

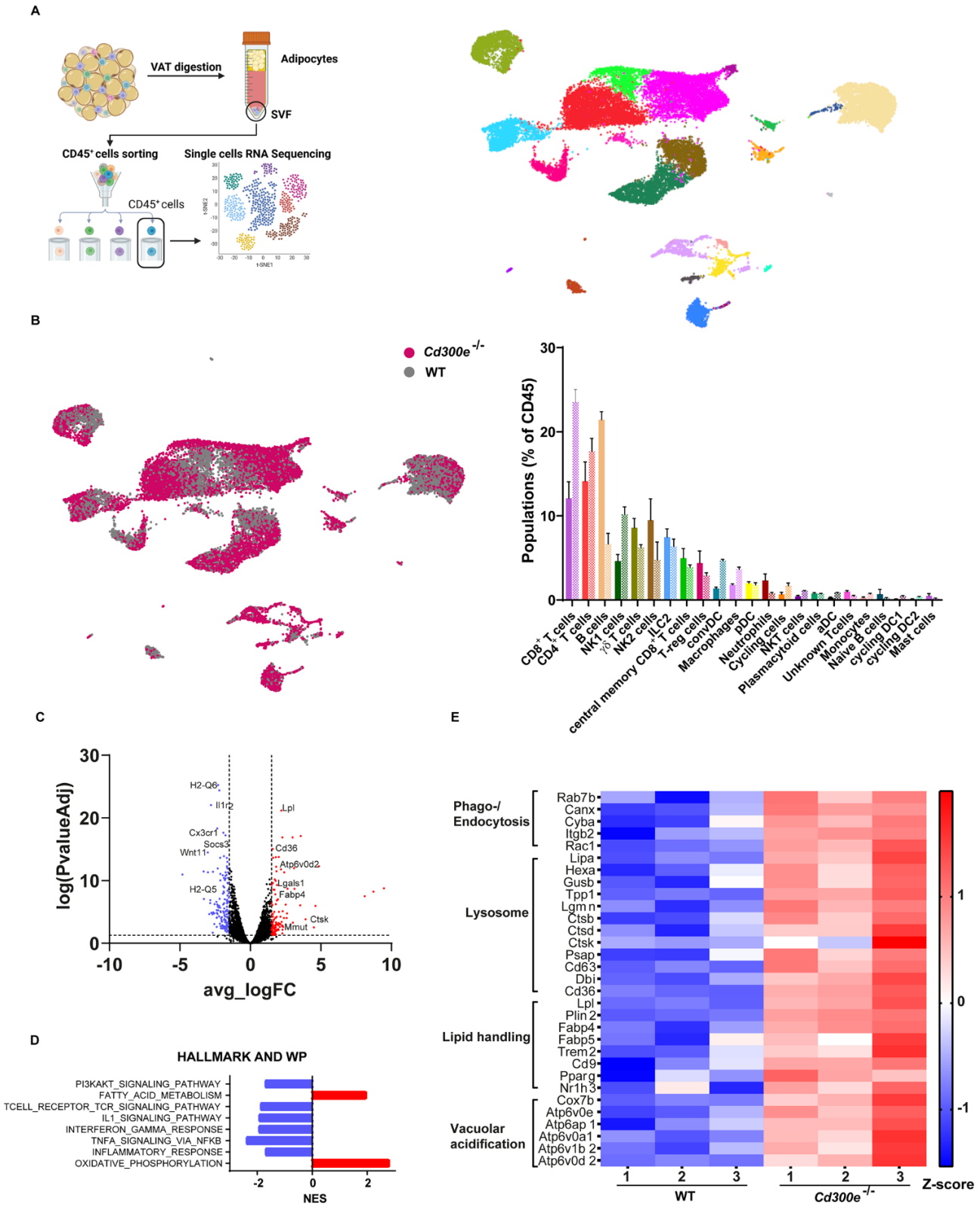
A
VAT digestion
Adipocytes
SVF
CD45⁺ cells sorting
Single cells RNA Sequencing
CD45⁺ cells
B
Cd300e -/-
WT
Populations (% of CD45)
CD8⁺ T cells
CD4⁺ T cells
B cells
NK1 cells
γδ T cells
NK2 cells
ILC2
central memory CD8⁺ T cells
T-reg cells
convDC
Macrophages
pDC
Neutrophils
Cycling cells
NKT cells
Plasmacytoid cells
aDC
Unknown T cells
Monocytes
Naive B cells
cycling DC1
cycling DC2
Mast cells
C
log(PvalueAdj)
avg_logFC
H2-Q6
Il1r2
Lpl
Cx3cr1
Socs3
Wnt11
Cd36
Atp6v0d2
Lgals1
Fabp4
H2-Q5
Ctsk
Mmut
D
HALLMARK AND WP
PI3KAKT_SIGNALING_PATHWAY
FATTY_ACID_METABOLISM
TCELL_RECEPTOR_TCR_SIGNALING_PATHWAY
IL1_SIGNALING_PATHWAY
INTERFERON_GAMMA_RESPONSE
TNFA_SIGNALING_VIA_NFKB
INFLAMMATORY_RESPONSE
OXIDATIVE_PHOSPHORYLATION
NES
E
Phago-/ Endocytosis
Lysosome
Lipid handling
Vacuolar acidification
Rab7b
Canx
Cyba
Itgb2
Rac1
Lipa
Hexa
Gusb
Tpp1
Lgmn
Ctsb
Ctsd
Ctsk
Psap
Cd63
Dbi
Cd36
Lpl
Plin2
Fabp4
Fabp5
Trem2
Cd9
Pparg
Nr1h3
Cox7b
Atp6v0e
Atp6ap 1
Atp6v0a1
Atp6v1b 2
Atp6v0d 2
WT
Cd300e -/-
Z-score

Figure 5. Single-cell characterization of the WT and *Cd300e*$^{-/-}$ VAT immune niche after diet-induced obesity. A) left panel: schematic workflow**.** WT or *Cd300e*$^{-/-}$ mice fed on HFD for 16 weeks were sacrificed (n=3 per group) and CD45^{+} cells were isolated by sorting from VAT and subjected to scRNA-Seq analysis. **Right panel**: cells were automatically clustered using the Louvain method. 24 distinct cell clusters are shown in reduced space generated through the uniform manifold approximation and projection (UMAP). Immune cell types were first annotated using the Azimuth method, and the classification was later refined through manual inspection of marker gene profiles. **B) left panel:** superimposition of WT and *Cd300e*$^{-/-}$ UMAP. **Right panel:** percentages of immune cell populations identified within total CD45^{+} cells in each condition were shown (WT mice are represented by filled bars, while *Cd300e*$^{-/-}$ mice are show by dotted bars). **C)** Volcano plot showing WT and *Cd300e*$^{-/-}$ mice gene expression fold change and their adjusted *p*-value. Dotted line divided significant genes (above, $p < 0.05$) from non-significant one (below, $p > 0.05$). Upregulated genes in *Cd300e*$^{-/-}$ mice compared to WT are indicated in red, while downregulated genes are labelled in blue. **D)** Enrichment analysis showing significantly different pathways compared between WT and *Cd300e*$^{-/-}$ mice after 16 weeks of HFD feeding. **E)** Heatmap representing genes belonging to lipid handling pathway that were differentially expressed between WT and *Cd300e*$^{-/-}$ mice fed on HFD. Data are represented as z-score (n=3/genotype). The differences between all represented genes are statistically significant ($p<0.05$).

Figure 6

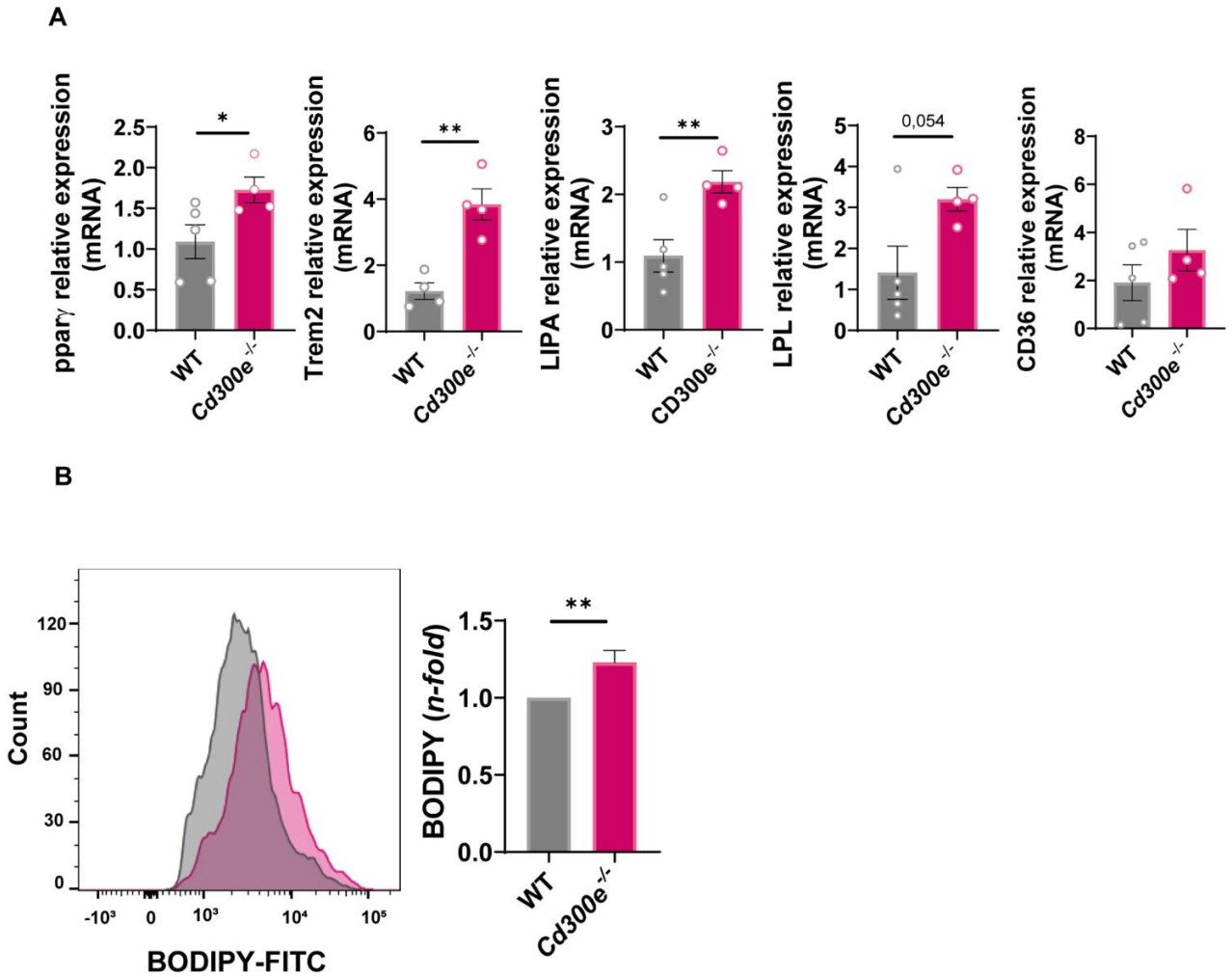

Figure 6. *Cd300e*$^{-/-}$ ATMs possess a LAM-like profile and accumulate more lipids. A) mRNA expression of ppar-γ, Trem2, LIPA, LPL and CD36 was evaluated by qRT-PCR on macrophages isolated from VAT of WT and *Cd300e*$^{-/-}$ mice after 16 weeks of HFD feeding. Data were normalized on 18S as endogenous reference genes and are expressed as $2^{-\Delta\Delta Ct}$ relative to WT mice. Data are expressed as mean ± SEM (WT, n=5; *Cd300e*$^{-/-}$, n=4). Statistical significance was determined by Student's t test. *, $p< 0.05$. P-values near the threshold for statistical significance are reported in the figure. **B) left panel:** representative histograms of Bodipy fluorescence in F4/80^{+} cells of VAT of WT and *Cd300e*$^{-/-}$ mice after 16 weeks of HFD feeding. WT and *Cd300e*$^{-/-}$ mice are shown in grey and purple, respectively. **Right panel:** Lipid content in F4/80^{+} cells infiltrating VAT was determined by BODIPY staining and quantified using flow cytometry. Data are expressed as mean ± SEM (n=11/genotype). Statistical significance was determined by Student's t test. **, $p< 0.01$.

Figure 7

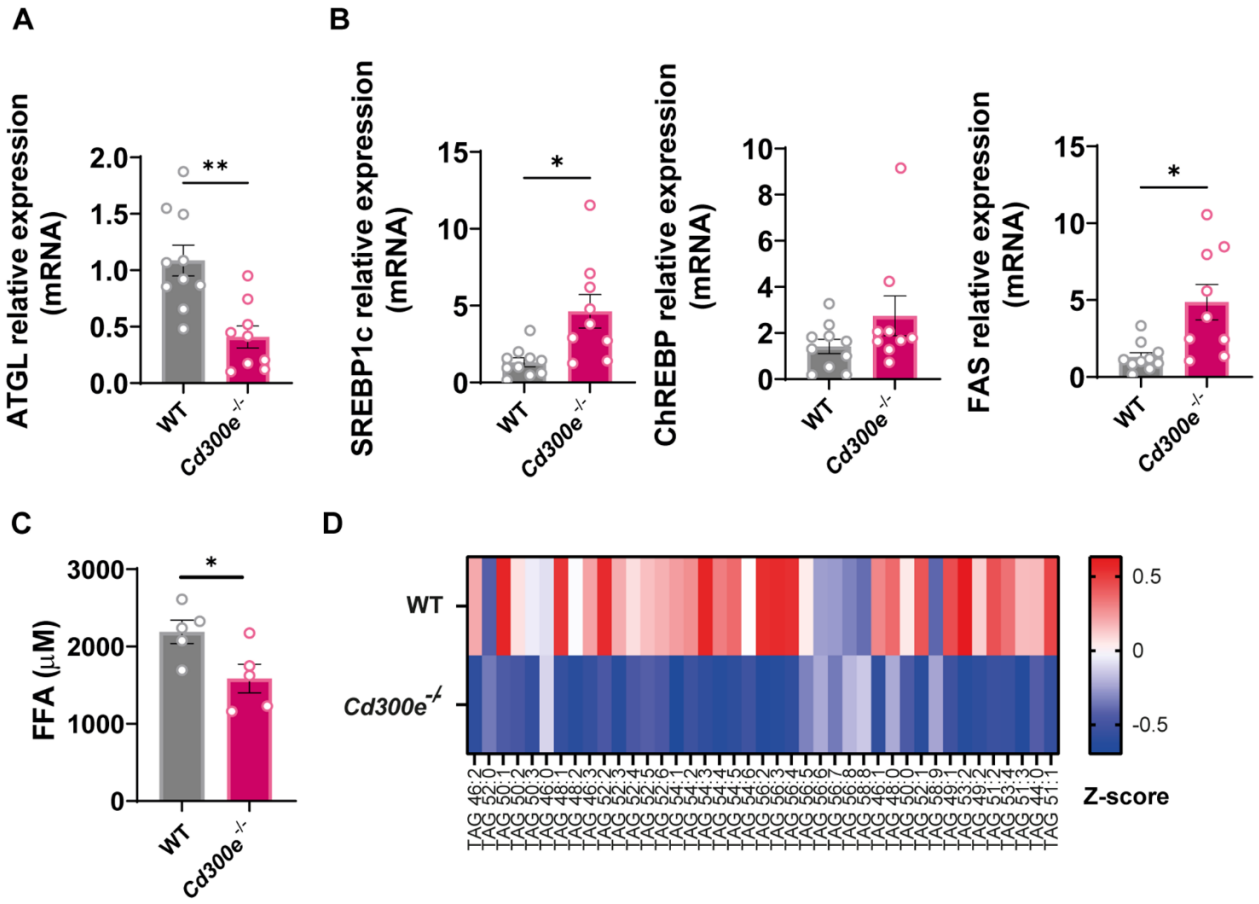

Figure 7. *Cd300e*$^{-/-}$ macrophages dampen adipocytes lipolysis and promote lipogenesis. A, B) mRNA expression of ATGL (**A**), SREBP1c, ChREBP and FAS (**B**) was evaluated by qRT-PCR on adipocytes isolated from VAT of WT and *Cd300e*$^{-/-}$ mice after 16 weeks of HFD feeding. Data were normalized on 18S as endogenous reference genes and are expressed as $2^{-\Delta\Delta Ct}$ relative to WT mice. Data are expressed as mean ± SEM (WT, n=10; *Cd300e*$^{-/-}$, n=9). Statistical significance was determined by Student's t test. *, $p< 0.05$; **, $p< 0.01$. **C)** FFA were quantified on plasma of WT and *Cd300e*$^{-/-}$ mice after 16 weeks of HFD feeding. Data are expressed as mean of µM (n=5/genotype). Statistical significance was determined by Student's t test. *, $p< 0.05$. **D**) Heat map visualizing phenotypes of TAG lipidomes detected in plasma of WT and *Cd300e*$^{-/-}$ mice after 16 weeks of HFD feeding. Data are expressed as mean of µM z-score (n=16/genotype).